Effects of Annealing Parameters on Optical Properties of Thermochromic VO2 Films Prepared in Aqueous Solution

ARTICLE *in* THE JOURNAL OF PHYSICAL CHEMISTRY C · JANUARY 2010

Impact Factor: 4.77 · DOI: 10.1021/jp909009w

7 AUTHORS, INCLUDING:

Litao Kang
Taiyuan University of Technology
29 PUBLICATIONS **708** CITATIONS

SEE PROFILE

Effects of Annealing Parameters on Optical Properties of Thermochromic VO_2 Films Prepared in Aqueous Solution

Litao Kang,[†,‡] Yanfeng Gao,[*,†] Zongtao Zhang,[†,‡] Jing Du,[†,‡] Chuanxiang Cao,[†,‡] Zhang Chen,[†,§] and Hongjie Luo[†]

Research Center for Industrial Ceramics, Shanghai Institute of Ceramics, Chinese Academy of Sciences, Dingxi 1295, Changning, Shanghai, 200050, China, Graduate University of Chinese Academy of Sciences, Yuquanlu 19, Beijing, 100049, China, and School of Materials Science and Engineering, Shaanxi University of Science and Technology, Xi'an, 710021, China

Received: September 17, 2009; Revised Manuscript Received: November 26, 2009

This work confirmed experimentally that the microstructure (grain boundaries, grain sizes, and size distributions) of VO_2 films has significant effects on the features of the semiconductor−metal (S−M) transition. This feature enables us to wisely regulate the parameters of the phase transition, which is of great importance in achieving practical applications. Thermochromic VO_2 films with various optical properties and phase transition parameters (for example: hysteresis widths ranging from 12 to 50 °C) have been synthesized on fused silica substrates via a simple solution process with inorganic precursors and polyvinylpyrrolidone (PVP). The widths and slopes of the hysteresis loops (i.e., the temperature sensitivity of the transition) can be regulated by controlling grain sizes and grain boundary conditions, which are believed to dominate the generation of the elementary hysteresis loop of each grain and the propagation of the S−M transition, respectively. A film consisting of qusai-isolated small particles shows a wide hysteresis loop due to the large interfacial energies and the lack of defects for nucleating. Besides, grain boundaries can decrease the interfacial energies and favor the phase propagation. In addition, particle sizes seem to influence the visible transmittances of these films effectively without deterioration of the infrared regulation ability. This experimental phenomenon is assigned to the blue shift of absorption edges (at around 500 nm) accompanying decreases in particle size.

1. Introduction

Vanadium dioxide, which shows a temperature-driven semiconductor−metal transition (S−M transition, critical temperature $T_c \approx 67$ °C), has intrigued researchers for the five decades since the first discovery of the existence of thermochromic properties.[1−5] Accompanying the S−M transition is a change of crystallographic structure, from monoclinic (M-phase, $P2_1/c$, semiconductor) at temperatures below T_c to tetragonal (R-phase, $P4_2/mnm$, metal) at temperatures above T_c.[2,6] The S−M transition is characterized by abrupt and dramatic changes in the electrical (typically 10^3-10^5 times in resistivity) and optical (up to 76% in near-infrared transmittance and up to 92% in infrared reflectance) properties,[1,7−11] suggesting applications in resistive switching elements, thermal relays, optical storage devices, holographic recording media, variable reflectivity mirrors, light modulators, smart windows, flat panel displays, etc.[12]

Significantly, the S−M phase transition occurs extremely fast and is completed in less than 500 fs for continuous VO_2 films.[13,14] Accordingly, Narayan and Bhosle proposed that the transformation is the result of a single coordinated jump of V cations.[15] Likewise, Klimov et al. assumed that the nuclei of R-phase VO_2 propagate in the M-phase VO_2 grain matrix with the acoustic velocity.[16] Therefore, it is widely believed that this S−M transition is a kind of martensitic transformation or at least has features in common with martensitic transformations.[16−18]

As in the case of martensitic transformations, the classical theory reveals that the thermal energy at T_c (∼67 °C, 2.9×10^{-2} eV) is much too small to overcome the energy barrier for homogeneous nucleation ($\sim 6/(T - T_c) \times 10^2$ eV, where $T - T_c$ represents superheating or undercooling, typically ≤25 °C).[17,18] As a result, nucleation at special sites (effective defects) must be preferable. A high concentration of effective defects leads to narrow hysteresis loops of S−M transitions, assuming that the size of crystal grains in the film is fixed.[17] On the basis of a similar theory, the effects of grain size on the S−M transition features of ultrathin polycrystalline VO_2 films are also interpreted.[19] These studies suggest that the features of the S−M transition are different for grains with different radii.[16,17,19] In fact, an inverse relationship between hysteresis widths and grain sizes has been anticipated when the grain size is less than a critical value (larger than 31 nm[19,20]). Small grains, as an effect of size reduction, seem to result in T_c depression and hysteresis broadening.[16] Therefore, compared to a bulk single crystal, the different features of hysteresis loops for polycrystalline VO_2 films are ascribed to the presence of a large number of various-sized VO_2 crystal grains.[16,21] Each crystal grain shows a vertical hysteresis loop with a defined height and a width, changing with grain sizes. The hysteresis loops in a measured area can be constructed by summing all the elementary loops of the grains in the area.[16,21]

Indeed, for free-standing single-crystalline VO_2 nanostructures or isolated nanoparticles on a Si substrate, the effect of size reduction on T_c depression and hysteresis broadening is convincingly reported.[22−24] Nevertheless, this effect seems to

* To whom correspondence should be addressed. E-mail: yfgao@mail.sic.ac.cn. Phone/Fax: +86-21-5241-5270.
† Chinese Academy of Sciences.
‡ Graduate University of Chinese Academy of Sciences.
§ Shaanxi University of Science and Technology.

10.1021/jp909009w
Published on Web 01/07/2010

be notably weakened for VO_2 aggregations/films consisting of grains with similar dimensions.[24−26] This phenomenon could be explained by the appearance of grain boundaries. According to the model proposed by Narayana and Bhosle,[15] aggregation of VO_2 particles through grain boundaries, especially textured and geometrically compatible grain boundaries, could reduce interfacial energy and thus depress the hysteresis loops.

Moreover, clear relationships between hysteresis loops and microscopic texture have already been clarified.[27,28] The degree of crystallographic misorientation between adjacent grains is reported to be related to the slope of the transition (the temperature sensitivity of the transition).[29,30] Well-matched grains make it possible to effectively propagate the metallic regions in the films without additional energy loss, and thus narrow the hysteresis widths while increasing the slopes of the S−M transition.[30] In contrast, the appearance of secondary or amorphous phases at the grain boundaries might result in hysteresis broadening.[31,32] Likewise, a similar hysteresis width change of 40 °C for VO_2 isolated nanoparticles and ∼10 °C for a continuous film was also reported,[24] suggesting that the influence of grain boundaries on hysteresis loops is very great. This significant influence of grain boundaries is further confirmed by the comparative Raman study of isolated VO_2 nanoparticles and contiguous VO_2 films.[23]

Experimentally, the nucleation and growth of R-phase VO_2 within the M-phase matrix have been directly observed with a scattering scanning near-field infrared microscope (s-SNIM).[4,33,34] It was found that a vast majority of the newborn R-phase VO_2 nuclei were located extremely close to grain boundaries (within ∼10 nm).[34] These nuclei grew and connected with increasing temperature.[4,34] These experimental results confirmed that T_c is area-selected in a VO_2 film; different microareas have different T_c values. The spread distribution of T_c among microareas would result in decreased slope of the corresponding phase transition curve with temperature,[21] as in the case of martensitic transformation for polycrystals.[35] Moreover, the percolative nature of the transition is also directly revealed.[4]

In summary, the VO_2 S−M transition occurs through a nucleation and propagation (or growth) process that is affected by microstructure defects, particle sizes, grain boundaries, and/or interfaces.[15−17,23,29−31,34] These effects of morphology on the S−M transition provide guidance to regulate the features of hysteresis loops. So far, many efforts have been made to tune the hysteresis widths and the slopes of individual branches.[8,24,31,36−39] However, some of these processes need high-temperature annealing (800−1000 °C) and special substrates (Al_2O_3 single crystals or fused silica);[8,36,37] the rest of the processes require post treatments, resulting in the shift of T_c, the appearance of a secondary phase, and/or the degradation of physical properties (reflectance or transmittance).[31,32,38,39]

Nevertheless, the ability to regulate hysteresis loops for VO_2 films, with an easy process, will eventually be needed for various practical applications.[24,36,40] For instance, sharp branches of hysteresis loops in electrical or optical properties mean high sensitivity, and narrow hysteresis loops imply good temperature responses between heating and cooling cycles. These features are inherently required for VO_2-based sensor-type devices.[15,40] On the other hand, a high reduction in infrared transmittance and a relatively wide hysteresis loop (15−20 °C) of near-infrared light are favorable when VO_2 is used as an optical storage medium.[15,24,36] Therefore, the development of a simple method to control the hysteresis loop features during VO_2 film synthesis is of great importance.[16]

In this paper, we report the successful preparation of thermochromic VO_2 films with controlled hysteresis loop features (widths and slopes) by optimizing the annealing parameters of films derived from an easy solution process. M/R-phase VO_2 films with different morphologies and/or hysteresis loops have been prepared by simply controlling annealing parameters, providing an effective process for growing high quality thermochromic VO_2 films with controllable hysteresis features. This controllability is simply introduced by control of polymer degradation rate through variation of annealing conditions, suggesting a general strategy to regulate film morphologies. Specifically, we addressed the effect of annealing on microstructures, and consequently on S−M transition and hysteresis loop parameters. Our results confirmed a recent finding that the nucleation of R-phase VO_2 in the M-phase matrix was closely related to grain boundaries[34] and further indicated that the state of grain boundaries influences effectively the S−M transition. On the basis of the results of a series of experiments, we have also addressed the relationship between the optical properties and the microstructure of the VO_2 films. We report an interesting phenomenon that the blue shift of the absorption edge near 500 nm occurred due to the decrease in particle sizes. This process is rather competitive for practical applications of VO_2 films because of its low cost, easy handling and ease for doping.[41]

2. Experimental Section

2.1. Starting Materials. Vanadium pentoxide (V_2O_5, analytically pure) and diamide hydrochloride ($N_2H_4 \cdot HCl$, analytically pure) were employed as starting materials to prepare a $VOCl_2$ solution. Polyvinylpyrrolidone (PVP, K90, average molecular weight: 1,300,000) was added as a film-forming promoter; all of these regents were bought from Sinopharm Chemical Reagent Co., Ltd., and used without further purification.

2.2. Preparation of Precursor Solution. Concentrated HCl (6 mL, 38%) solution and a solution containing 1 g of $N_2H_4 \cdot HCl$ were added into an aqueous suspension (20 mL) containing 3.5 g of V_2O_5. After being warmed while stirring, a blue solution formed. The solution was treated with a small amount of V_2O_5 or $N_2H_4 \cdot HCl$ until it contained no VO_2^+ and V^{3+} and was then filtered and a clear $VOCl_2$ solution (pH ≈ 1) was obtained. The concentration of the $VOCl_2$ solution was adjusted to 0.1 $mol \cdot L^{-1}$ and PVP (K90, average molecular weight: 1,300,000) was added to the solution in gravimetrically determined proportions (6 wt %). This was used as the precursor solution for VO_2 coating. The detailed manufacturing procedure for the $VOCl_2$ solution can be found in literature.[42]

2.3. Preparation of Films. Films were coated on the fused silica substrates by spin coating at 400 rpm for 6 s and then 3000 rpm for 30 s. After drying at 60 °C for 10 min to drive off the excess solvent, a smooth thin film of VO_2 precursor was formed. After annealing at a certain temperature for a fixed time in nitrogen flow, the obtained precursor gel films were crystallized into thermochromic VO_2.

Caution: vanadium precursors are highly toxic. Contact may irritate skin, eyes, and mucous membranes. It may be toxic by ingestion, inhalation, and skin absorption. Effects of contact or inhalation may be delayed.

2.4. Characterization. Morphologies of the films were determined by JSM-6700F field emission scanning electron microscopy (FESEM) and JEM-2010 transmission electron microscopy (TEM). Thermochromic switching parameters were monitored on a Hitachi U-4100 UV−visible−NIR spectrophotometer equipped with a film heating unit in the wavelength

TABLE 1: Annealing Conditions and the Designations of Corresponding Films

sample	temperature (°C)	time (min)	heating rate (°C·min^{-1})	film thickness (nm)
I	600	5	30	88
II	600	20	30	102
III	600	60	30	98
IV	600	180	30	83
V	500	20	30	98
VI	500	60	30	103
VII	500	180	30	84
VIII	500	180	3	100

range of 240 to 2600 nm. Temperature was measured with assistance of a PT100 temperature sensor in contact with the films and was controlled via a temperature controlling unit. The temperature errors were less than ±1.5 °C based on repeating measurements. Hysteresis loops were measured by collecting the transmittance of films at a fixed wavelength (2000 nm) at approximately 2.0 °C intervals. Transmittance spectra before and after phase transition were recorded at 30 and 90 °C on the heating semicycles. Reflectance spectra were recorded at only 30 °C on the heating semicycles. X-ray diffraction (XRD) was carried out on a XPERT-PRO X-ray diffractometer using Cu Kα radiation with a grazing angle of 0.5°. Raman spectroscopy was measured on a Renishaw invia Raman microscope spectrometer using a 514.5 nm laser at a laser output power of 2 mW. The wavelength of the instrument was calibrated before each measurement.

3. Results and Discussion

For convenience of discussion, the annealing conditions, the designations of corresponding films and the thicknesses of these films have been listed in Table 1. The thickness of film was determined by optical spectra using the following relationship:

$$nd = {}^{k\lambda}/_{2}$$

where n, d, and λ represent the refractive index, film thickness, and wavelength of the antireflection valley in reflectance spectra. The data on n are adapted from the literature.[43] The value of k is a constant for a certain antireflection valley. In the case of our films, there is just one antireflection valley for each reflectance spectrum. As a result, the value of k should be 1. The half wave loss at the interface of the air/VO_2 film has been taken into account in the equation. The result reveals that the thicknesses of these films, 93 ± 10 nm, are comparable. It should be emphasized that the film thickness determined in this way is an assumed optical thickness rather than the real film thickness. However, it is believed that this optical thickness is more advisible than the real film thickness, because this film was porous. It cannot reflect the porosity difference among samples and sometimes it is also difficult to determine the real film thickness due to both the roughness of the surfaces and pores of the films.

In a previous work, we reported the successful development of a novel process for the preparation of M/R-phase VO_2 thin films with cheap inorganic vanadium(IV) precursors. XRD and Raman spectra have confirmed the formation of VO_2 in pure M/R-phase.[41] Optical characterizations for these samples also reveal significant transmittance changes in the infrared region for all the samples (about 50% at 2000 nm), which is comparable

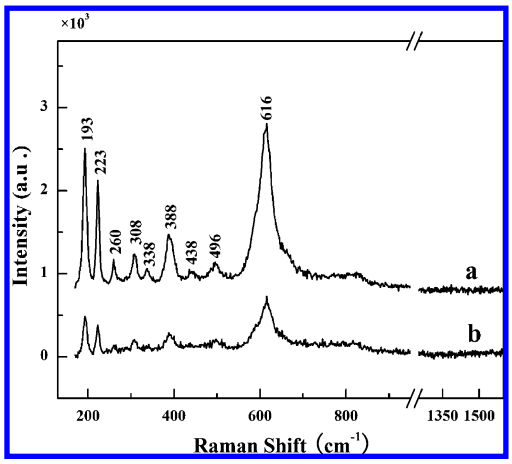

Figure 1. Raman spectra for samples IV (a) and V (b) with an output power of 2 mW.

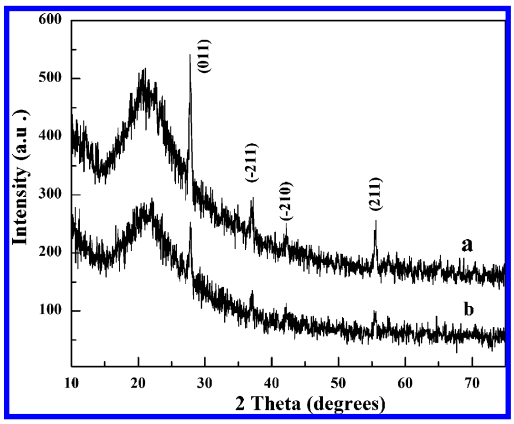

Figure 2. XRD spectra for samples III (a) and IV (b) with a grazing angle of 0.5°.

to that reported.[44−46] The excellent thermochromic properties suggest that our VO_2 films are of high quality.

To further confirm the phase purity of these films, Raman and XRD spectrometries were performed on typical films and the Raman analysis results (samples IV and V) have been exhibited in Figure 1. The bands agree well with the reported data for M-phase VO_2, with centers at 193 [192,[47] 195,[48] 191[49]], 223 [223,[47] 222,[48] 221[49]], 260 [261,[47] 264,[48] 258[49]], 308 [310,[47] 304,[48] 308[49]], 338 [338,[48] 335[49]], 388 [390,[47] 392],[48,49] 438 [439[48]], 496 [500,[47] 496,[48] 497[49]], 616 [622,[48] 612],[48,49] and 816 [825[48]] cm^{-1}. The absence of bands for any impurities, such as V_2O_5 phase with Raman shifts at around 700 and 994 cm^{-1} or disordered/graphite carbon with Raman shifts at around 1320 and 1591 cm^{-1},[50,51] indicates that there are no significant amounts of relative impurities. The different strength of Raman shifts between samples IV and V was attributed to differences in crystallinity.

The XRD spectra (samples III and IV, Figure 2) further verified the phase purity of M-phase VO_2. All of the peaks in these spectra can be indexed to M-phase VO_2 (JCPDS card no. 72−0514, $P21/c$, a = 0.5743 nm, b = 0.4517 nm, c = 0.5375 nm, and β = 122.61°). A broad amorphous background peak, which stretches from 10 to 35°, is attributed to the fused silica substrates.

Figure 3 shows typical SEM photos of VO_2 films heated at 600 °C for different times with a heating rate of 30 °C·min^{-1} (samples I−IV). All the films are porous, consisting of irregular particles. The pore formation is attributed to the degradation of PVP and the shrinkage of the gel film during annealing.[41] Grain

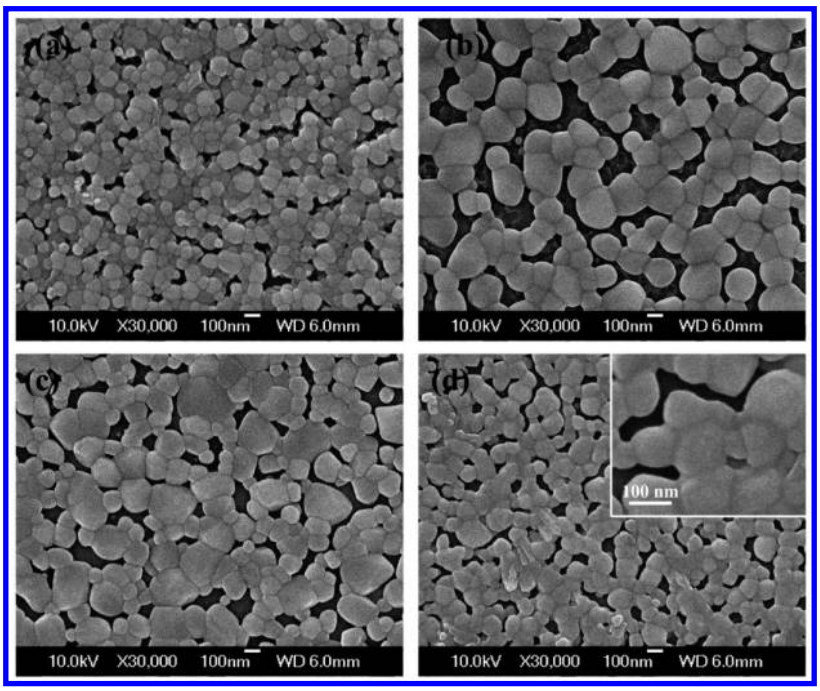

Figure 3. SEM photos of sample I (a), sample II (b), sample III (c), and sample IV (d). Samples were obtained by annealing at 600 °C for different times, 5 min (a), 20 min (b), 60 min (c), and 180 min (d) with heating rate of 30 °C·min^{-1}. The inset of photo d is a high-resolution SEM photo of sample IV.

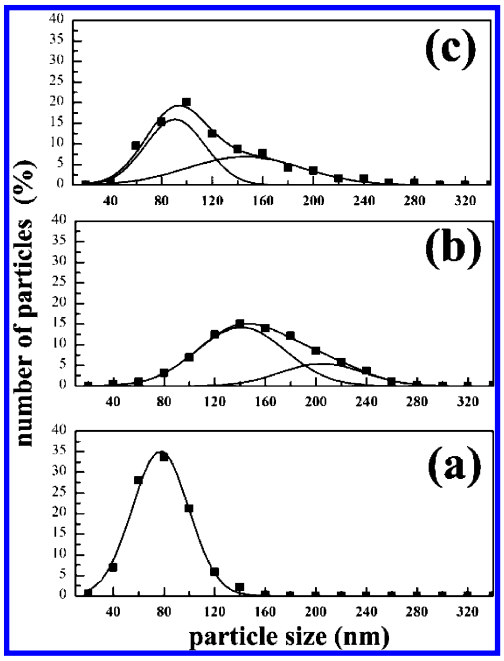

Figure 4. Scatter graphs showing the particle size distributions in sample I (a), sample II (b), and sample III (c). The solid curves are those after fitting by Gaussian distribution. Samples were obtained by annealing at 600 °C for different times, 5 min (a), 20 min (b), and 60 min (c) with heating rate of 30 °C·min^{-1}.

boundaries change from clear (parts a−c of Figure 3) to fuzzy (inset in Figure 3d) as the annealing time is prolonged. Meanwhile, the particle size varies dramatically, associated with distinct change of porosity and pore shape. To evaluate the differences of particle size among samples, the distributions of particle sizes was measured. The corresponding size distribution scatter graph as well as fitting curves with Gaussian distribution is shown in Figure 4. The scatter graphs were plotted by randomly measuring the dimensions of 300 grains in a given micrograph. The particle size distribution scatter graphs of Figure 3d failed to be obtained due to fuzzy grain boundaries. The results showed that the grain size of sample I complied with Gaussian distribution, while the distributions for samples II and III distinctly exhibited two maxima. The size distribution scatter graphs indicated that when annealing time increases from 5 to 20 min, the particle size increases rapidly (parts a and b of both Figures 3 and 4). However, the VO_2 particles shrink noticeably for the long time annealing samples (Figure 4c and parts c and d of Figure 3), resulting in few large particles and a broad distribution of particle sizes. The shrinkage of particle size (which is also observed in the 500 °C annealed films) and change of grain boundaries are tentatively attributed to the mass transport via surface diffusion during annealing. This mass transport has been reported as the main reason for morphology evolution of VO_2 films during the heat treatment of predeposited amorphous ones at 450 °C.[24]

When the S−M transition of VO_2 occurs, it exhibits an abrupt transmittance change in the infrared region. As a result, a hysteresis loop of transmittance−temperature appears on the heating/cooling cycles. The typical optical transmittance spectra and hysteresis loops of these VO_2 films (at 2000 nm wavelength) have been collected and shown in Figure 5. The parameters of these hysteresis loops are obtained as follows.

From the transmittance (Tr)−temperature (T) data, a plot of d(Tr)/d(T) − T is obtained, yielding one or two peaks with well-defined maxima (see Figure 6). Each of the d(Tr)/d(T) − T curves has been fitted with a Gaussian function using the peak fitting module of Originpro 7.5 software. The temperature corresponding to the maximum d(Tr)/d(T) is defined as the phase transition temperature (T_c) of the branch ($T_{c,h}$ and $T_{c,c}$ represent T_c of heating and cooling branches, respectively). For cooling branches, the appearance of steps introduces two peaks in the d(Tr)/d(T) − T curves. The T_c values of these branches are determined by the main peaks. The slope of the transition is expressed by the full width at half-maximum (fwhm) of the peak. The width of the hysteresis loop, ΔT_c, is defined as the

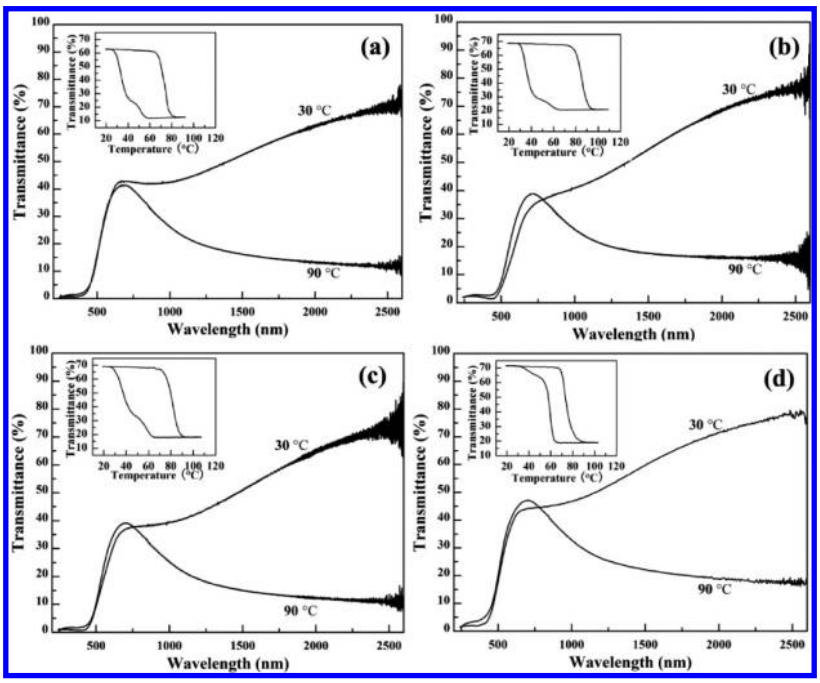

Figure 5. Optical transmittance spectra and temperature dependence of optical transmittance (insets) at a fixed wavelength (2000 nm) for sample I (a), sample II (b), sample III (c), and sample IV (d). Samples were obtained by annealing at 600 °C for different times, 5 min (a), 20 min (b), 60 min (c), and 180 min (d) with heating rate of 30 °C·min^{-1}.

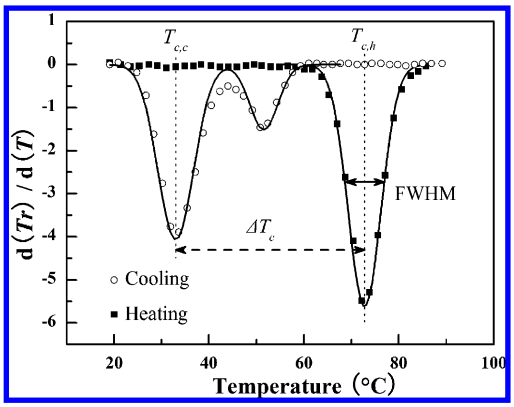

Figure 6. A schematic description of the definition of the S−M transition parameters for heating and cooling branches using the d(Tr)/d(T) − T plot (corresponding to the sample I in Figure 3 and Table 1). T and Tr represent temperature and transmittance at wavelength of 2000 nm. The resulting parameters $T_{c,h}$, $T_{c,c}$, ΔT_c, and fwhm of peaks are employed to express phase transition temperature of heating, cooling branches, the width of the hysteresis loop, and the slope of the transition, respectively.

temperature difference of $T_{c,h} - T_{c,c}$. The parameters of the phase transition for these films have been summarized in Table 2.

The widths of the hysteresis loops are 39.8, 50, and 45.3 °C for samples I, II, and III, respectively. These widths are much larger than the typical values for continuous polycrystalline VO_2 films (10−15 °C,[9] 3−20 °C,[24] 6−18 °C,[52] 8−15 °C[53]) but are consistent with isolated VO_2 nanoparticles or with films composed of isolated nanoparticles (30−50 °C,[17] 18 ± 2 °C and 56 ± 5 °C,[23] 38 °C,[24] 30 and 35 °C[54]). The main factors that affect the S−M transition are crystallinity, grain size, and grain boundaries.[22,24,29] Prolonged annealing should improve crystallinity, resulting in hysteresis loop broadening.[24] For samples I−IV, however, no obvious similar relationship is found, indicating that crystallinity is not the principal factor affecting hysteresis loops. In fact, a series of experiments revealed that after annealing at 400 °C, the thermochromic property began to appear, suggesting the formation of M/R-phase VO_2 crystallites. The thermochromic property would be improved with increasing temperature and kept almost unchanged at temperatures above 450 °C. This result is in good agreement with the crystallization temperatures of VO_2 (≤450 °C[24] and 370−410 °C[42]). For these thin films, annealing at 600 °C for relatively long times has very limited effects on the film crystallinity. The effect of grain size, which is believed to determine an elementary hysteresis loop,[16] also seems unable to explain the differences in hysteresis loops. In general, the grain size of VO_2 increases with prolonging annealing time.[24] In this case, the hysteresis width should decrease, and sample III should show the narrowest hysteresis loop of all.[16,19] These predictions are obviously different from our results. If we regard the particles in SEM photos as the monomeric units that determine hysteresis loops, as what was proposed in the literature,[23] sample II should exhibit narrowest hysteresis loop

TABLE 2: Parameters of the S−M Transition in Samples I−IV[a]

	transition temperature T_c (°C)			transmittance at 2 μm (%)			fwhm		
sample	heating	cooling		30 °C	90 °C	Hysteresis width ΔT_c (°C)	heating	cooling	
I	72.8	**51.5**	33.0	62.5	13.1	39.8	8.1	**7.0**	8.9
II	85.0	**57.7**	35.0	68.7	15.9	50.0	9.8	**10.0**	7.5
III	81.8	**58.8**	36.5	69.3	18.6	45.3	9.3	**7.4**	12.0
IV	73.0	**38.0**	59.3	71.4	18.7	13.7	6.7	**12.5**	6.1

[a] The bold letters indicate the parameters of the small peak on cooling branches of the d(Tr)/d(T) − T plot.

among samples I−IV. This is also not the case of our experiments.

On the basis of these analyses, the dominating factor that influence ΔT_c is deduced to be the states of the grain boundaries. The current films present the different states of grain boundaries: continuous or discrete and crystallized or amorphous. Adjacent grains typically have different orientations and/or a layer of poorly crystallized phases. These states limit the propagation of a new phase, usually leading to large hysteresis loops.[15,29] Among the three samples, most of the grains in sample II are connected linearly (Figure 3b). In the other two samples, a grain usually connects with several other grains (parts of a and c of Figure 3). This difference suggests that there are more imperfections such as grain boundaries and crevices that favor the R-phase VO_2 nucleation[34] and propagation in samples I and III. Consequently, samples I and III show relatively narrow widths. This deduction is in line with various experimental results,[23,24] and it is also compatible with the effect of grain size proposed by Lopez et al.[17] It should be pointed out that Lopez et al. studied samples consisting of isolated VO_2 nanoparticles. Only limited effects of grain boundary were taken into consideration.

Sample IV, in contrast, exhibits a much narrower hysteresis loop (13.7 °C), in good accord with the typical values for continuous polycrystalline VO_2 films.[9,24,52] Meanwhile, there is an obvious fwhm decrease of the heating branch, i.e., the phase transition becomes sensitive to temperature changes (Table 2). These experimental phenomena suggest dramatic changes of grain boundaries and a notable improvement of phase transition propagation among grains for sample IV.[15,29,30] In this film, superheating (or undercooling) induces the S−M (or M−S) transition to occur first in preferable nucleation sites, and then these nuclei propagate through grain boundaries, as was observed by Qazilbsh et al.[4,34] The propagation of the S−M transition through grain boundaries promotes the phase transition of connected grains at relatively low driving forces, resulting in a significant shift of $T_{c,h}$ and $T_{c,c}$ to the thermodynamic equilibrium temperature (∼67 °C, see in Table 2). We believe that the grain boundaries in sample IV (Figure 3d) developed, coalesced, and crystallized well after a long annealing time.

Significantly, obvious steps were observed at the cooling branches for samples I, II, and III (insets of parts a−c of Figure 5, annealing for 5, 20, and 60 min, respectively). The appearance of steps suggests another loop width, as indicated in Table 2. The steps are resulted from a difference in temperature of inhomogeneous occurrence of phase transition in the films due to the two-humped grain size distributions (parts b and c of Figure 4)[16] or the site-selective nucleation of product phase, as observed in literature.[34] However, there are also some contradictions. First, this deduction is difficult to explain the step appearing in sample I, which manifests a Gaussian distribution with one maximum in grain size. Second, this deduction suggests that the temperatures of the $d(Tr)/d(T) - T$ peaks should vary as the size distribution changes. For sample II and III, however, although the size distribution curves are quite different (parts b and c of Figure 4), the step appears at similar temperatures on the cooling branch of the $d(Tr)/d(T) - T$ curves. Therefore, it seems that these experiment results do not agree to the model suggested by Klimov et al.[16] In fact, the propagation of the phase transition through grain boundaries may possibly counteract inhomogeneous distribution of T_c in the VO_2 films. Therefore, there is usually no step observed in relatively narrow hysteresis loops.[19,32] It is believed that any models related to the steps in the hysteresis loops should take the influence of grain boundary into account.

For sample IV (annealed for 180 min), the step seems to be depressed (inset of Figure 4d). This result could be explained by the coalescence of grain boundaries and the improvement of phase transition propagation through grain boundaries, which would push the step upward. The appearance of the step in only one of the two branches is associated with the asymmetry of the elementary hysteresis loops (i.e., the loops assigned to individual grains) with respect to the phase equilibrium temperature.[32] The asymmetry of the elementary hysteresis loops, in turn, is attributed to a transition temperature shift accompanying with a decrease in grain size,[22,23] or with stress at the substrate/film interface.[32,55]

To further clarify the effects of grain size on the widths of hysteresis loops, films with similar morphologies and relatively homogeneous size distribution are needed. The current solution process enables us to achieve widely morphology control. In previous research, we have revealed that the precursor solution is in a state of solution rather than sol. After the solvent evaporation, the interactions among polymer molecules, along with those between the carbonyl groups and the metal ions, ensure the formation of cross-linked high quality gel films.[41] In these films, the metal ions are bonded with the polymer through electrostatic interactions, forming a uniform organic−inorganic hybrid precursor film.[56−58] The formation of metal oxide occurs after degradation of polymer begins.[41,57] Therefore, the morphologies of final films could be easily controlled via adjusting the degradation rate of polymers. Meanwhile, for crystallization in a solid-state reaction, the dependence of nucleation and growth rate on temperature is usually different.[59] Thus, it is expected that the morphologies of VO_2 films could be tailored by variations of heat treatments. Accordingly, the films have been prepared under the same synthesis conditions as samples I−IV but at an annealing temperature of 500 °C.

Typical SEM photos and optical transmittance spectra, along with the hysteresis loops, are shown in Figure 7. The parameters of the S−M transition for these films (samples V−VII, Table 1) have been summarized in Table 3. The sample obtained by annealing at 500 °C for 5 min showed a bluish color but almost no thermochromic properties and is excluded.

Films produced at this annealing temperature have similar morphologies (parts a−c of Figure 7). Compared to films obtained by annealing at 600 °C, in which many quasi-isolated grains appear, all of these films show grains tightly connected across boundaries. The grain sizes are smaller than those treated at 600 °C. The film obtained by annealing for 20 min (sample V) consists of connected, irregular particles (Figure 7a). Typically, the largest dimension of each particle is around 100 nm. These particles possess flat surfaces, indicating that the mass transport during annealing is feeble for a short annealing time. The film produced by annealing for 60 min (sample VI) shows similar granular morphologies with a relatively large roughness, and the particle size is reduced notably (Figure 7b). Prolonging the annealing time to 180 min (sample VII) results in increases in porosity and surface roughness (Figure 7c), indicating the enhancement in mass transport that changes the surface morphology of these particles.[24,59]

From Table 3, it is clearly revealed that the hysteresis widths of these films are narrower than those of films annealed at 600 °C (Table 2). This change in loop width can be attributed to the decreased grain size and the grain boundary continuity (Figure 7). The hysteresis width of sample VI is 38% lower than that of sample VII. As seen in the SEM photos (Figure 7), the particle sizes of these two samples are similar, and thus should have limited influence on hysteresis loops. This differ-

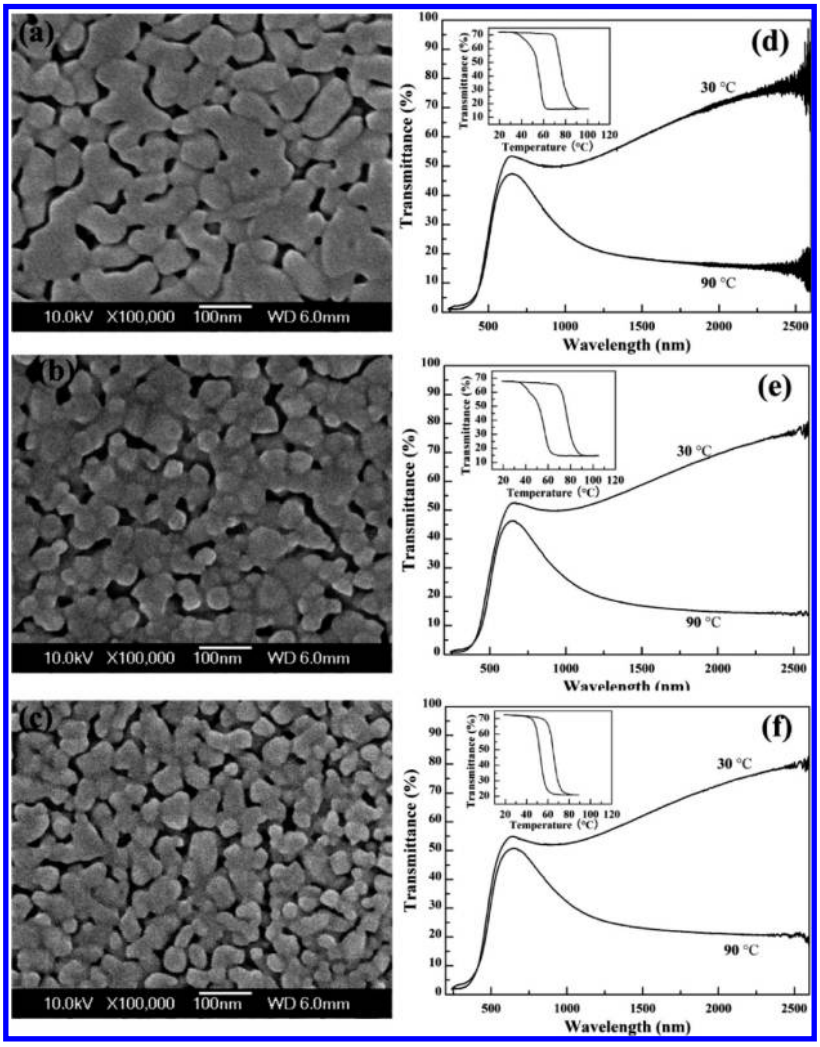

Figure 7. SEM photos and optical transmittance spectra of samples V (a and d), VI (b and e), and VII (c and f). Insets show corresponding hysteresis loops at 2000 nm. Samples were obtained by annealing at 500 °C for different times, 20 min (a and d), 60 min (b and e), and 180 min (c and f). Heating rate is the same, 30 °C·min^{-1}.

TABLE 3: Parameters of the S−M Transition of Samples V, VI, and VII[a]

	transition temperature T_c (°C)			transmittance at 2 μm (%)			fwhm		
sample	heating	cooling		30 °C	90 °C	hysteresis width ΔT_c (°C)	heating	cooling	
V	74.8	**56.4**	42.1	70.8	16.6	18.4	9.8	**7.1**	12.2
VI	76.5	**56.5**	41.5	69.5	14.9	20.0	9.8	**8.6**	11.0
VII	65.2		52.8	72.7	21.2	12.4	9.0		8.4

[a] The bold letters indicate the parameters of the small peak on cooling branches of the d(Tr)/d(T) − T plot.

ence is attributed to the coalescence of grain boundaries by mass transport, which may improve the propagation of phase transition, as in the case of sample IV.[15,29,30]

The heating rate is also expected to have an effective influence on the morphology of VO_2 films and consequently on the S−M transition. At a relatively low heating rate, the degradation of polymer and the release of product gases proceed slowly. Meanwhile, the number density of nuclei should increase due to the relatively long duration at temperatures suitable for VO_2 nucleation, producing tiny VO_2 nuclei and a large number of grain boundaries. The surface energy of these tiny VO_2 nuclei is very large and thus tends to reduce by coalescing into large crystallites. To study the influence of heating rate, a film (sample VIII) was prepared by heating at 500 °C for 180 min with a rate of 3 °C·min^{-1}. The SEM photos and the corresponding optical transmittance spectra and hysteresis loops are shown in Figure 8. The corresponding S−M transition parameters are listed in Table 4.

It is shown that sample VIII consisted of interconnected particles and irregular pores. The sharp branches of the hysteresis loops (inset of Figure 8b) confirm the effective propagation of S−M transition through grain boundaries.[15] In fact, the slope of the S−M transition (fwhm = 4.1 °C) is comparable with that of epitaxial VO_2 films (fwhm = 3.1 °C).[30] Significantly, the hysteresis width of sample VIII is similar to that sample VII, which was prepared at 500 °C with a heating rate of 30 °C·min^{-1}, but the fwhm of sample VII (9.0 °C) is much larger. The large fwhm of sample VII should be attributed to the spread distribution of $T_{c,c}$ and $T_{c,h}$.

To further verify our discussion on grain boundaries, two films (sample I and sample VIII) were scraped off from their substrates and observed by TEM (Figure 9).

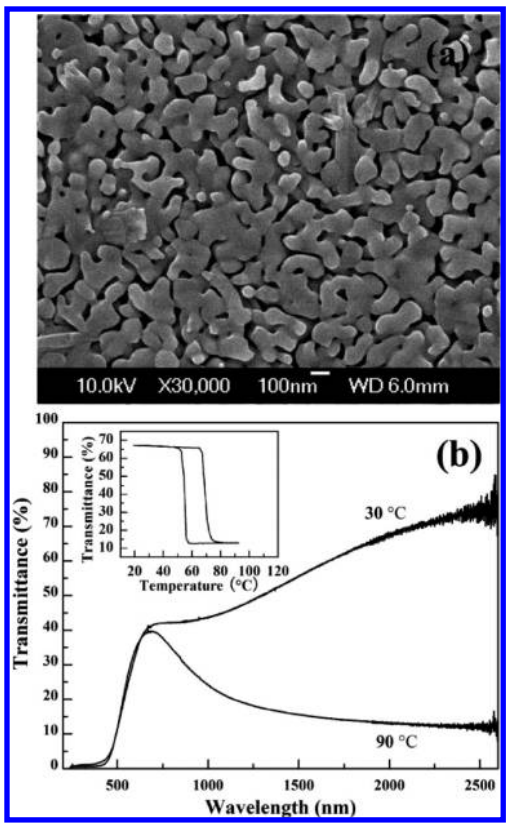

Figure 8. SEM photos and optical transmittance spectra of sample VIII (a and b). Samples were obtained by annealing at 500 °C (a and c) for 180 min with heating rate of 3 °C·min^{-1}. Inset of b shows corresponding hysteresis loops at 2000 nm.

Parts a−c of Figure 9 present TEM photos of sample I. It is shown that the sample is assembled from irregular particles. Distinct grain boundaries are observed in high resolution TEM photos (parts a−c of Figure 9), indicating that the grain boundaries are very loose in this film. The Fourier transform (FFT) patterns of corresponding crystal grains (Figure 9 insets) reveal diffraction spots, verifying the crystallinity. Significantly, the diffraction spots in the FFT patterns become hazy or disordered in the vicinity of grain boundaries. This experimental phenomenon can be ascribed to the poor crystallization of VO_2 under short annealing time (600 °C, 5 min). Generally, spaces about 2−5 nm in width were observed between grains, and they were attributed to poorly crystallized phases and/or voids. It is widely reported that VO_2 films with second or amorphous phases at grain boundaries demonstrate a broadened hysteresis, which is definitely consistent with our experiments.[17,31,36,54]

Sample VIII, on the other hand, consisted of smooth connected particles and interconnected pores among particles (parts d and e of Figure 9). This morphology should be a result of mass transport and aggregation of the primary VO_2 crystals during annealing.[24] The high magnification TEM photo clearly demonstrates that the grain boundaries are very sharp (Figure 9f). In fact, it seems that the lattice fringes pass though grain boundaries. The FFT patterns (Figure 9f insets) of the corresponding crystal grains are composed of two groups of bright diffraction spots, confirming the existence of boundaries and the high crystallinity of these crystals. The TEM photos are fully consistent with the SEM results (Figures 3a and 8a) and the deductions from optical measurements (Figure 5a inset and Figure 8b inset).

To evaluate the optical and thermochromic properties of the samples, the integral transmittances of films annealed with heating rate of 30 °C·min^{-1} were calculated in the visible region (380−780 nm), so were the integral infrared transmittance reduction before and after the S−M phase transition in the wavelength of 1500 − 2500 nm. The results are shown in Figure 10.

According to the theory suggested by Narayan and Bhosle,[15] the amplitude of the transition should deteriorate as the defect content increases. It is expected that the 500 °C annealed samples should be less crystallized and thus contain high defect content. Accordingly, they should exhibit deteriorated infrared transmittance reduction compared with the 600 °C annealed samples. This phenomenon was not obviously detected in our films, even though the hysteresis widths of the films vary considerably. In fact, it is clearly revealed that the 500 °C annealed samples show better visible transmittance than those annealed at 600 °C, while the infrared transmittance reduction remains comparable. For instance, the infrared transmittance reduction of sample VI (53.8%, 500 °C, 60 min annealed sample) is a little larger than that of sample II (51.2%, 600 °C, 20 min annealed sample). Meanwhile, the integral visible transmittance of sample VI (34.5%) is much higher than that of sample II (20.2%).

To explain the differences in the optical properties between these films, hemispherical reflectance spectra of samples II and VI were collected from 240 to 2600 nm (Figure 11). It was found that the integral hemispherical reflectance of sample VI (18.7%) was 3.5% larger than that of sample II (15.2%) in the visible region. Because both of the integral transmittance and integral reflectance for sample II are smaller than those of sample VI in the visible region, one can conclude that the absorption and/or scattering of sample II are much larger. The hemispherical transmittance of the sample was recorded, in order to eliminating the influence of scattering. It was still shown that both the hemispherical transmittance and the hemispherical reflectance of sample II are less than those of sample VI in the visible region, indicating that the absorption of sample II is larger than that of sample VI (Figure 12). In fact, from the transmittance spectra of sample II and sample VI (Figure 5b and Figure 7e), it is clearly revealed that the optical absorption edges (at about 500 nm wavelength) of these samples are different. The optical absorption edge of VO_2 could be represented by λ^* (the maximum of the $d(Tr)/d\lambda - \lambda$ curves for the semiconductor phase). The values of λ^* for all samples have been determined and the results along with optical properties (integral visible transmittance, reflectance in a region of 380 − 780 nm and integral infrared transmittance reduction in a region of 1500−2500 nm) are listed in Table 5.

It is found that the change of λ^* seems to be correlated to the particle size in films. For example, samples II and III, the particles of which were the largest among these samples, manifest λ^* of longest wavelength. In contrast, samples VI and VII with the smallest particles show λ^* in the shortest

TABLE 4: Parameters of the S−M Transition of Sample VIII

	transition temperature T_c (°C)		transmittance at 2 μm (%)			fwhm	
sample	heating	cooling	30 °C	90 °C	hysteresis width ΔT_c (°C)	heating	cooling
VIII	68.9	54.7	67.4	13.2	14.2	4.1	3.4

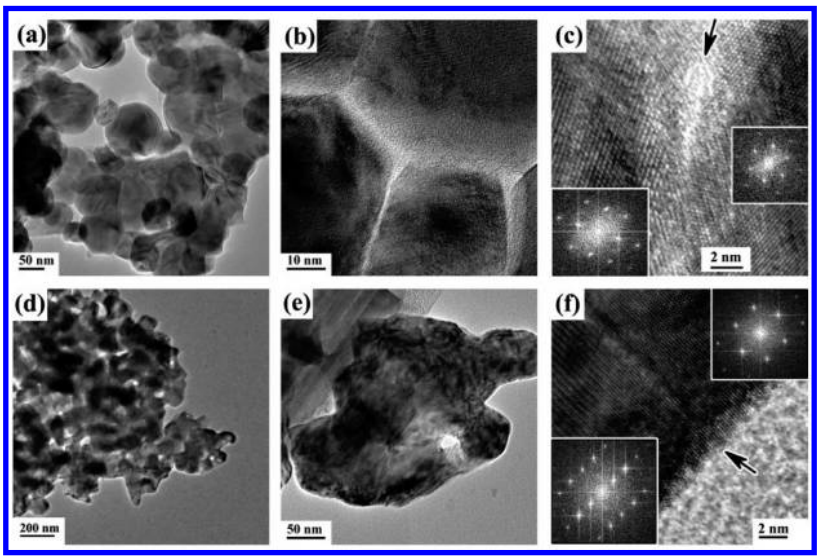

Figure 9. TEM photos of sample I (a, b, and c) and sample VIII (d, e, and f). The insets of photos c and f are FFT patterns of corresponding crystal grains. Samples were obtained by annealing at 600 °C for 5 min (a, b, and c) with a heating rate of 30 °C·min^{-1}, and 500 °C for 180 min (d, e, and f) with a heating rate of 3 °C·min^{-1}, respectively.

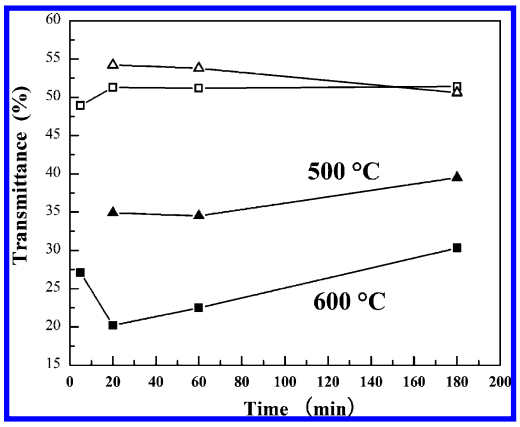

Figure 10. Integral visible transmittance (in a region of 380−780 nm, filled polygons) and integral infrared transmittance reduction (in a region of 1500−2500 nm, open polygons) of films annealed at 600 °C (squares, samples I−IV) and 500 °C (triangles, samples V−VII) with heating rate of 30 °C·min^{-1}.

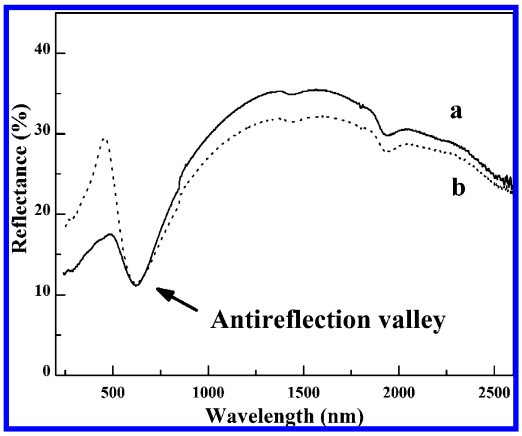

Figure 11. Reflectance spectra of sample II (a) and sample VI (b). Samples were obtained by annealing at 600 °C for 20 min (a) and 500 °C for 60 min (b) with heating rate of 30 °C·min^{-1}.

wavelength. The regulating ability of the absorption edges is of importance in tailoring the visible optical properties of VO_2 films, because this absorption edge effectively influences the color and the visible transmittance.[60]

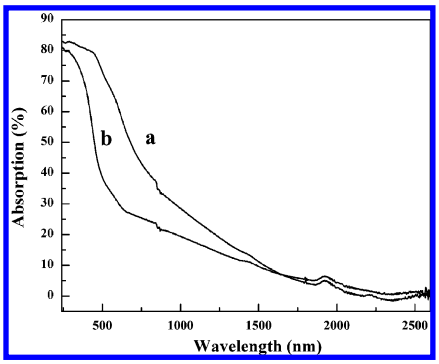

Figure 12. Absorption spectra of sample II (a) and sample VI (b). Samples were obtained by annealing at 600 °C for 20 min (a) and 500 °C for 60 min (b) with heating rate of 30 °C·min^{-1}.

This absorption edge could be attributed to electronic transitions between the O2p$_\pi$ valence band and the conduction band[60,61] or more precisely a potential convolution of two or more electronic transitions.[62] For F-doped VO_2 films, a very good correlation between the absorption edge shift and spectral weight variation of O2p valence band was observed,[60,63] verifying the relationship between energy band structure and the absorption edge.

Numerous factors could introduce energy band structure variation and ultimately variations in performance (amplitudes and slopes of the transition, electronic properties), including V−O stoichiometry, finite-size effects, and the electronic inhomogeneity near surfaces.[20,25,64] First, the energy band structure changes accompanying V−O stoichiometry are closely related to the amplitude of the S−M transition. VO_2 compounds with very similar stoichiometry would exhibit different energy band structure and completely miss the transition.[64] In our experiments, dramatic S−M transitions are observed in all the films, and the infrared transmittance reductions are comparable, indicating that the V−O stoichiometry is very close to 1:2 and weakly influences the energy band structure.

Second, it is reported that the electronic properties near surfaces of VO_2 are different from those in the interior,[25] which

TABLE 5: Visible Transmittance, Reflectance, Infrared Transmittance Reduction and λ^* Determined by Optical Measurements

sample	I	II	III	IV	V	VI	VII	VIII
visible transmittance (%)	27.1	20.2	22.5	30.3	34.9	34.5	39.5	24.5
visible reflectance (%)	12.8	15.2	18.1	21.4	18.7	19.0	17.4	15.2
infrared transmittance reduction (%)	48.9	51.2	51.3	51.4	54.2	53.8	50.6	53.2
λ^* (nm)	490	566	520	499	491	475	470	513

may introduce variations in energy band structure. However, the electronic inhomogeneity of VO_2 surfaces is in a region within a few lattice constants of VO_2; consequently, "surface-sensitive" technologies (scanning tunneling spectroscopy and photoemission) are always needed to detect the inhomogeneity.[25,65] Spectrophotometry is not a "surface-sensitive" technology and should reflect the result of average optical properties including both surfaces and bulk. Thus, this kind of inhomogeneity is unlikely to affect the absorption edges significantly.

Finite-size effects might play a very important role in the energy band structure variation and subsequent shift of absorption edges. As noted above, several reports have indicated that the features of the S−M phase transition (temperatures and hysteresis widths) can be varied strongly by controlling the crystallite/particle size.[22,23] Moreover, Kim et al. have reported the variation of band gap energy (between the conduction band bottom and the valence band top for the semiconductor phase) from about 0.77 to 0.57 eV when they reduced the VO_2 film thickness from 31 to 6 nm.[20] We note that the size and the change in band gap energy reported for finite-size effects are comparable with those of our films.[20,22,23] Therefore, it is possibe that the shift of absorption edges is a consequence of finite-size effects.

Besides the variation of energy band structure, the morphologies of films may also affect the optical properties. For example, the increase in porosity of VO_2 films results in a decrease of absorption coefficient (α), refractive index (n), and extinction coefficient (k). For direct optical transitions, the corresponding energy gap could be determined by the $(\alpha h\nu)^2 - h\nu$ curves. Thus, it is reasonable to expect that the porosity of VO_2 films would influence α and then the energy gap, introducing a shift of absorption edge. At the same time, the variation of n and k will also change the value of reflectance according to the relationship $R = ((n-1)^2 + k^2)/((n+1)^2 + k^2)$. Further studies are carrying out and possibly could provide insights into the relationship between particle sizes and the absorption edges.

4. Conclusions

The effects of annealing conditions (annealing temperatures, time, and heating rate) on the morphology of VO_2 films were systemically studied by means of SEM, TEM, and UV−visible−NIR spectrophotometry. It was found that the annealing conditions markedly influence the film morphology and consequently the parameters of the S−M transition. This feature enables us to deliberately regulate the parameters of the S−M transition of thermochromic VO_2 films obtained via a simple solution process. The variation of S−M transition parameters is mainly ascribed to different grain boundary conditions and grain sizes, which are believed to determine the elementary hysteresis loop of each grain and the propagation of the S−M transition across grain boundaries. It is found that loose grain boundaries limit the propagation of the S−M transition, resulting in a large width of hysteresis. Meanwhile, the site-selective nucleation produces a distribution of $T_{c,c}$, which could introduce a difference of temperature for inhomogeneous occurrence of phase transition and a step on the cooling branch of the hysteresis loop. Significantly, an obvious blue shift of absorption edge (at about 500 nm) with a decrease of particle size was discovered. Further studies are needed to explain this experimental phenomenon.

Acknowledgment. This study was supported in part by the Century Program (One-Hundred-Talent Program) of the Chinese Academy of Sciences, National Key Basic Research Project (NKBRP, 2009CB939900), the National Natural Science Foundation of China (NSFC, Contract No. 50772126), Shanghai Key Basic Research Project (09DJ1400200), and Shanghai Basic Research Project (08JC1420300).

References and Notes

(1) Morin, F. J. *Phys. Rev. Lett.* **1959**, *3* (1), 34–36.
(2) Goodenough, J. B. *J. Solid State Chem.* **1971**, *3*, 11.
(3) Takahashi, Y.; Kanamori, M.; Hashimoto, H.; Moritani, Y.; Masuda, Y. *J. Mater. Sci.* **1989**, *24* (1), 192–198.
(4) Qazilbash, M. M.; Brehm, M.; Chae, B. G.; Ho, P. C.; Andreev, G. O.; Kim, B. J.; Yun, S. J.; Balatsky, A. V.; Maple, M. B.; Keilmann, F.; Kim, H. T.; Basov, D. N. *Science* **2007**, *318* (5857), 1750–1753.
(5) Cao, C. X.; Gao, Y. F.; Luo, H. J. *J. Phys. Chem. C* **2008**, *112* (48), 18810–18814.
(6) Kim, B. J.; Lee, Y. W.; Choi, S.; Lim, J. W.; Yun, S. J.; Kim, H. T.; Shin, T. J.; Yun, H. S. *Phys. Rev. B* **2008**, *77* (23), 235401.
(7) Barker, A. S.; Verleur, H. W.; Guggenheim, H. J. *Phys. Rev. Lett.* **1966**, *17* (26), 1286.
(8) Gea, L. A.; Boatner, L. A. *Appl. Phys. Lett.* **1996**, *68* (22), 3081–3083.
(9) Nag, J.; Haglund, R. F. *J. Phys.-Cond. Matter.* **2008**, *20* (26), 264016.
(10) Guinneton, F.; Sauques, L.; Valmalette, J. C.; Cros, F.; Gavarri, J. R. *Thin Solid Films* **2004**, *446* (2), 287–295.
(11) Ruzmetov, D.; Zawilski, K. T.; Senanayake, S. D.; Narayanamurti, V.; Ramanathan, S. *J. Phys.-Cond. Matter.* **2008**, *20* (46), 465204.
(12) Gurvitch, M.; Luryi, S.; Polyakov, A.; Shabalov, A.; Dudley, M.; Wang, G.; Ge, S.; Yakovlev, V. *J. Appl. Phys.* **2007**, *102* (3), 033504.
(13) Cavalleri, A.; Tóh, C.; Siders, C. W.; Squier, J. A.; Ráksi, F.; Forget, P.; Kieffer, J. C. *Phys. Rev. Lett.* **2001**, *87* (23), 237401.
(14) Cavalleri, A.; Dekorsy, T.; Chong, H. H. W.; Kieffer, J. C.; Schoenlein, R. W. *Phys. Rev. B* **2004**, *70* (16), 161102.
(15) Narayan, J.; Bhosle, V. M. *J. Appl. Phys.* **2006**, *100* (10), 103524.
(16) Klimov, V. A.; Timofeeva, I. O.; Khanin, S. D.; Shadrin, E. B.; Ilinskii, A. V.; Silva-Andrade, F. *Tech. Phys.* **2002**, *47* (9), 1134–1139.
(17) Lopez, R.; Haynes, T. E.; Boatner, L. A.; Feldman, L. C.; Haglund, R. F. *Phys. Rev. B* **2002**, *65* (22), 224113.
(18) Kaufman, L.; Cohen, M. *Progress in Metal Physics*; Chalmers, B., King, R., Eds.; Pergamon Press: New York, 1958; Vol. 7, pp 165−246.
(19) Aliev, R.; Andreev, V.; Kapralova, V.; Klimov, V.; Sobolev, A.; Shadrin, E. *Phys. Solid State* **2006**, *48* (5), 929–934.
(20) Kim, H. K.; You, H.; Chiarello, R. P.; Chang, H. L. M.; Zhang, T. J.; Lam, D. J. *Phys. Rev. B* **1993**, *47* (19), 12900–12907.
(21) Danilov, O. B.; Klimov, V. A.; Mikheeva, O. P.; Sidorov, A. I.; Tul'skii, S. A.; Shadrin, E. B.; Yachnev, I. L. *Tech. Phys.* **2003**, *48* (1), 73–79.
(22) Whittaker, L.; Jaye, C.; Fu, Z. G.; Fischer, D. A.; Banerjee, S. *J. Am. Chem. Soc.* **2009**, *131* (25), 8884–8894.
(23) Donev, E. U.; Lopez, R.; Feldmant, L. C.; Haglund, R. F. *Nano Lett.* **2009**, *9* (2), 702–706.
(24) Suh, J. Y.; Lopez, R.; Feldman, L. C.; Haglund, R. F. *J. Appl. Phys.* **2004**, *96* (2), 1209–1213.
(25) Chang, Y. J.; Yang, J. S.; Kim, Y. S.; Kim, D. H.; Noh, T. W.; Kim, D. W.; Oh, E.; Kahng, B.; Chung, J. S. *Phys. Rev. B* **2007**, *76* (7), 075118.
(26) Peng, Z. F.; Jiang, W.; Liu, H. *J. Phys. Chem. C* **2007**, *111* (3), 1119–1122.
(27) Haidinge, W.; Gross, D. *Thin Solid Films* **1972**, *12* (2), 433–438.
(28) Petit, C.; Frigerio, J. M.; Goldmann, M. *J. Phys.-Cond. Matter.* **1999**, *11* (16), 3259–3264.

(29) Denatale, J. F.; Hood, P. J.; Harker, A. B. *J. Appl. Phys.* **1989**, *66* (12), 5844–5850.
(30) Chae, B. G.; Kim, H. T.; Yun, S. J.; Kim, B. J.; Lee, Y. W.; Youn, D. H.; Kang, K. Y. *Electrochem. Solid State Lett.* **2006**, *9* (1), C12–C14.
(31) Aliev, R. A.; Andreev, V. N.; Klimov, V. A.; Lebedev, V. M.; Nikitin, S. E.; Terukov, E. I.; Shadrin, E. B. *Tech. Phys.* **2005**, *50* (6), 754–757.
(32) Aliev, R. A.; Klimov, V. A. *Phys. Solid State* **2004**, *46* (3), 532–536.
(33) Qazilbash, M. M.; Brehm, M.; Andreev, G. O.; Frenzel, A.; Ho, P. C.; Chae, B. G.; Kim, B. J.; Yun, S. J.; Kim, H. T.; Balatsky, A. V.; Shpyrko, O. G.; Maple, M. B.; Keilmann, F.; Basov, D. N. *Phys. Rev. B* **2009**, *79* (7), 075107.
(34) Frenzel, A.; Qazilbash, M. M.; Brehm, M.; Chae, B. G.; Kim, B. J.; Kim, H. T.; Balatsky, A. V.; Keilmann, F.; Basov, D. N. *Phys. Rev. B* **2009**, *80* (11), 115115.
(35) Ortin, J.; Planes, A.; Delaey, L. *Hysteresis in Shape-Memory Materials*; Elsevier: London, 2005; Vol. 3, pp 467−553.
(36) Lopez, R.; Boatner, L. A.; Haynes, T. E.; Haglund, R. F.; Feldman, L. C. *Appl. Phys. Lett.* **2001**, *79* (19), 3161–3163.
(37) Gea, L. A.; Budai, J. D.; Boatner, L. A. *J. Mater. Res.* **1999**, *14* (6), 2602–2610.
(38) Andreev, V.; Kapralova, V.; Klimov, V. *Phys. Solid State* **2007**, *49* (12), 2318–2322.
(39) Case, F. C. *J. Vac. Sci. Technol. A* **1984**, *2* (4), 1509–1512.
(40) Jin, P.; Yoshimura, K.; Tanemura, S. *J. Vac. Sci. Technol. A* **1997**, *15* (3), 1113–1117.
(41) Kang, L.; Gao, Y.; Luo, H. *ACS Appl. Mater. & Interfaces* **2009**, *1* (10), 2211–2218.
(42) Zheng, C. M.; Zhang, J. L.; Luo, G. B.; Ye, J. Q.; Wu, M. M. *J. Mater. Sci.* **2000**, *35* (13), 3425–3429.
(43) Kakiuchida, H.; Jin, P.; Tazawa, M. *Sol. Energy Mater. Sol. Cells* **2008**, *92* (10), 1279–1284.
(44) Binions, R.; Hyett, G.; Piccirillo, C.; Parkin, I. P. *J. Mater. Chem.* **2007**, *17* (44), 4652–4660.
(45) Maaza, M.; Bouziane, K.; Maritz, J.; McLachlan, D. S.; Swanepool, R.; Frigerio, J. M.; Every, M. *Opt. Mater.* **2000**, *15* (1), 41–45.
(46) Lee, M.-H.; Cho, J.-S. *Thin Solid Films* **2000**, *365* (1), 5–6.
(47) Manning, T. D.; Parkin, I. P.; Clark, R. J. H.; Sheel, D.; Pemble, M. E.; Vernadou, D. *J. Mater. Chem.* **2002**, *12* (10), 2936–2939.
(48) Kim, H. T.; Chae, B. G.; Youn, D. H.; Kim, G.; Kang, K. Y.; Lee, S. J.; Kim, K.; Lim, Y. S. *Appl. Phys. Lett.* **2005**, *86* (24), 242101.
(49) Petrov, G. I.; Yakovlev, V. V.; Squier, J. *Appl. Phys. Lett.* **2002**, *81* (6), 1023–1025.
(50) Gurvitch, M.; Luryi, S.; Polyakov, A.; Shabalov, A.; Dudley, M.; Wang, G.; Ge, S.; Yakovlev, V. J. Appl. Phys. 2007, *102* (3).
(51) Pol, V. G.; Pol, S. V.; Calderon-Moreno, J. M.; Gedanken, A. *J. Phys. Chem. C* **2009**, *113* (24), 10500–10504.
(52) Chen, S. H.; Ma, H.; Dai, J.; Yi, X. J. *Appl. Phys. Lett.* **2007**, *90* (10), 101117.
(53) Saeli, M.; Binions, R.; Piccirillo, C.; Parkin, I. P. *Appl. Surf. Sci.* **2009**, *255* (16), 7291–7295.
(54) Sidorov, A. I.; Vinogradova, O. P.; Obyknovennaya, I. E.; Khrushchova, T. A. *Tech. Phys. Lett.* **2007**, *33* (7), 581–582.
(55) Muraoka, Y.; Hiroi, Z. *Appl. Phys. Lett.* **2002**, *80* (4), 583–585.
(56) Luo, H. M.; Jain, M.; McCleskey, T. M.; Bauer, E.; Burrell, A. K.; Jia, Q. X. *Adv. Mater.* **2007**, *19* (21), 3604–3607.
(57) Jia, Q. X.; McCleskey, T. M.; Burrell, A. K.; Lin, Y.; Collis, G. E.; Wang, H.; Li, A. D. Q.; Foltyn, S. R. *Nat. Mater.* **2004**, *3* (8), 529–532.
(58) Burrell, A. K.; McCleskey, T. M.; Jia, Q. X. *Chem. Commun.* **2008**, (11), 1271–1277.
(59) Kingery, W. D. *Introduction To Ceramics*; John Wiley and Sons, Inc.: New York, 1960.
(60) Burkhardt, W.; Christmann, T.; Franke, S.; Kriegseis, W.; Meister, D.; Meyer, B. K.; Niessner, W.; Schalch, D.; Scharmann, A. *Thin Solid Films* **2002**, *402* (1−2), 226–231.
(61) Gavini, A.; Kwan, C. C. Y. *Phys. Rev. B* **1972**, *5* (8), 3138–&.
(62) Qazilbash, M. M.; Schafgans, A. A.; Burch, K. S.; Yun, S. J.; Chae, B. G.; Kim, B. J.; Kim, H. T.; Basov, D. N. *Phys. Rev. B* **2008**, *77* (11), 115121.
(63) Burkhardt, W.; Christmann, T.; Meyer, B. K.; Niessner, W.; Schalch, D.; Scharmann, A. *Thin Solid Films* **1999**, *345* (2), 229–235.
(64) Ruzmetov, D.; Senanayake, S. D.; Narayanamurti, V.; Ramanathan, S. *Phys. Rev. B* **2008**, *77* (19), 195442.
(65) Yin, W.; West, K. G.; Lu, J. W.; Pei, Y.; Wolf, S. A.; Reinke, P.; Sun, Y. *J. Appl. Phys.* **2009**, *105* (11), 114322.

JP909009W